nature communications

Article

https://doi.org/10.1038/s41467-024-51621-1

Directed crystallization of a poly(3,4-ethylenedioxythiophene) film by an iron(III) dodecyl sulfate lamellar superstructure

Received: 21 September 2023

Accepted: 14 August 2024

Published online: 16 September 2024

Check for updates

Feng Ma[1,7], Sang-il Choi[1], Dooyong Lee[2], Sung Bae Jeon[1], Sungkyun Park[3], Sung-Pyo Cho[4,5], Jin-Hyo Boo[6] & Sungsoo Kim[1]

Poly(3,4-ethylenedioxythiophene):polystyrene sulfonate (PEDOT:PSS), a successfully commercialized polymeric semiconductor material, has potential as a transparent electrode in flexible electronic devices, yet has insufficient conductivity. We present the synthesis, properties, and directed crystallization of the PEDOT:dodecyl sulfate (PEDOT:DS) film. Iron(III) dodecyl sulfate ($Fe(DS)_3$) multi-lamellar vesicles (MLVs), a new growth template, are used to synthesize and direct the growth of the PEDOT:DS film via vapor-phase polymerization of 3,4-ethylenedioxythiophene to form huge PEDOT:DS co-crystal domains within the MLV superstructure. The polycrystalline film has metallic conductivity (avg. ~1.0×10^4 S cm^{-1}), is highly transparent and mechanically durable yet flexible, and suitable for next-generation flexible electronics. These noteworthy properties are conferred by the MLV lamellar superstructure of $Fe(DS)_3$, a selective oxidant and an efficient in situ dopant that enhances the film hydrophobicity and durability. Sophisticated MLV-type oxidants are foreseen to enable the synthesis of more conductive, transparent, robust, flexible, and water-stable polymer electrode materials in future.

Poly(3,4-ethylenedioxythiophene) (PEDOT) is a highly attractive material for use as a transparent electrode in flexible electronic devices such as organic light-emitting diodes (OLEDs), smart batteries, supercapacitors, solar cells, and biosensors. The attractiveness of PEDOT can be attributed to the fact that most of the technological factors governing the practical applicability of this material, i.e., the film casting process, transparency, flexibility, cost, etc., are highly competitive in terms of commercialization even though its electrical conductivity, mechanical durability, and stability in water could still be further improved[1]. For example, PEDOT doped with polystyrene sulfonate (PEDOT:PSS), the most intensively studied and successfully commercialized polymeric semiconductor material, has hardly been investigated as a real substitute for a representative transparent electrode such as indium tin oxide (ITO). This is because of the insufficient conductivity of a pristine PSS-doped PEDOT film, which is only 800 S cm^{-1} at most[2], largely attributable to the inherent limitation in the form of massive barriers created by the insulating PSS dopants within the film. Accordingly, many studies have been carried out to improve the conductivity, some of which entailed pre- and post-treatment of the film with polar organic solvents or strong acids, e.g., ethylene glycol (EG)[3], dimethyl sulfoxide (DMSO)[4], H_2SO_4[2,5,6], and HNO_3[7]. Several notable studies have shown that these solvents or acids could considerably enhance the conductivity to as much as 4000 – 6000 S cm^{-1} [7,6]. However, these treatments are highly likely to destabilize the film, mostly because of the dissociation and eventual removal of the massive PSS barriers from within the film[8]. Moreover,

[1]Department of Materials Engineering, Paichai University, Daejeon, Korea. [2]Department of Physics Education, Kyungpook National University, Daegu, Korea. [3]Department of Physics, Pusan National University, Busan, Korea. [4]National Center for Inter-University Research Facilities, Seoul National University, Seoul, Korea. [5]Graphene Research Center, Advanced Institute of Convergence Technology, Suwon, Korea. [6]Department of Chemistry, Sungkyunkwan University, Suwon, Korea. [7]Present address: School of Chemistry and Materials Engineering, Hunan University of Arts and Science, Changde, Hunan Province, China. e-mail: skim@pcu.ac.kr

the conductivity of PEDOT is likely to be distinctly lower after treatment with a hydrophilic solvent during a subsequent process and/or long-term exposure to water in air. This is because the relatively small dopant ions that substitute the bulky polymer anions would be readily de-doped[8].

Along with these efforts to improve the conductivity of the PEDOT:PSS film, other researchers endeavored to develop a highly conductive and high-quality PEDOT film by adding dopants other than the PSS anion[9]. The most notable film-casting method toward this goal is vapor-phase polymerization (VPP)[10]. Other methods, such as electropolymerization (EP)[11], solution casting polymerization (SCP)[12], and chemical vapor deposition (CVD)[13] have also received considerable attention. With the exception of the EP method, which requires a conductive substrate that limits its practical application in flexible electronic devices, the SCP[12], CVD[13], and VPP[14] methods have produced noteworthy results with regard to the film quality and conductivity at the micrometer scale, both of which are essential properties for its application as a flexible transparent electrode (FTE). On the other hand, it is important to note that the use of all of these methods to reach the maximum conductivity required the aid of various additives (or basic inhibitors) and additional dopants to supplement the methods with pre-, mid-, or post-treatments. The addition of a basic inhibitor during the polymerization of EDOT is intended to suppress the reactivity and crystallization of the overly acidic Fe(III) oxidant to render the film highly conductive and homogeneous[15]. Unfortunately, the basic inhibitor itself, which exists inside the PEDOT film, is known to prevent further growth of the crystal domains, thereby further limiting the potential increase in the conductivity[16]. Another reason for the treatment of the PEDOT film with additional dopants or strong acids is the insufficient and/or inefficient doping of the cationic polymer backbones by the counter-anions from the oxidants during polymerization. Therefore, it seems reasonable to think that these approaches have a clear limitation. A more efficient as well as effective oxidant that would entirely obviate the need for inhibitors and additional dopants during polymerization but would ensure that the resulting film is highly conductive, would certainly be more desirable.

In fact, a similar concept was proposed by Shi et al.[17] who used iron(III) dodecylbenzenesulfonate ($Fe(DBSA)_3$) as oxidant as well as dopant-supplier to prepare a high-quality PEDOT film via self-inhibited polymerization. This means that VPP could be used without the addition of any inhibitor or secondary dopant. Their study produced the first example of a highly conductive PEDOT thin film ($\sigma = 1100\ S\ cm^{-1}$) polymerized with the Fe(III) cation and then doped with its counter anion comprising a surfactant with a long hydrocarbon-tail. This surfactant-type iron salt is partly similar to the aforementioned new kind of oxidant in the sense that it is inhibitor-free. However, the benzene moiety of the DBSA anion is suspected to prevent the anion from effectively and intimately doping the cationic PEDOT backbone. This is probably due to the strong steric hindrance introduced by the bulky functional group, despite the ability of the group to serve as a basic electron-donating inhibitor during VPP. Thus, it is logical to deduce that the resultant film is less conductive than would otherwise be possible. To verify this hypothesis, trials with trivalent salts of various long and single hydrocarbon-tailed anionic surfactants without a benzene group as a self-inhibited oxidant seemed to be a good starting point.

This motivated our study, which started with an assessment of various types of Fe(III) salts of anionic surfactants with different chain lengths and head groups (listed in Supplementary Table 1). All these trivalent iron oxidants were prepared in highly pure form from the commercially available Na salts of the anionic surfactants via simple anion exchange by dissolving $FeCl_3$ in methanol. We analyzed a total of seven different trivalent iron oxidants to verify their feasibility for VPP. Among them, only three different Fe(III) oxidants, those with n-octyl carboxylate, n-dodecyl sulfate, and n-dodecyl sulfonate anions, respectively, were soluble in various alcohols to form a clear solution for possible VPP implementation. We subsequently discovered that the VPP-PEDOT film grown using Fe(III) n-dodecyl sulfate (DS) has surprisingly high electrical conductivity (~ $4000\ S\ cm^{-1}$) even in the first trial, whereas that of the film grown using Fe(III) n-dodecyl sulfonate is ~ $1000\ S\ cm^{-1}$. Therefore, we decided to focus on $Fe(DS)_3$ as a self-inhibited oxidant as well as a dopant-supplier to synthesize a high-quality PEDOT film by using the VPP method. VPP-PEDOT films doped with dodecyl sulfate ions were systematically prepared under a number of different conditions, whereupon they were scrupulously analyzed with various powerful analytical tools to identify the conditions that would yield the most optimal characteristics, i.e., electrical conductivity, light transmittance, water stability, and mechanical durability. In addition, the polymer films were prepared on various substrates, such as polyethylene terephthalate (PET), polyimide (PI), glass, and an oxidized Si-wafer, to assess their broad applicability. To our surprise, the quality and properties of these films were found to be nearly identical, and markedly superior to those of any conductive polymer film ever reported.

Results and discussion

Synthesis and thermal property of iron(III) dodecyl sulfate

Unlike extensively studied anionic surfactants, such as sodium or lanthanum dodecyl sulfate[18,19], iron(III) dodecyl sulfate is not well studied because it has not attracted much interest from academics except for use as an iron(III) catalyst in organic synthesis[20,21]. However, although the oxidizing capability of $Fe(DS)_3$ has been proven to be highly selective and efficient, as verified by its performance as a catalyst, only very few studies[22,23] concerned with its use as an oxidant, particularly for the oxidative polymerization of conductive polymers, have been reported. The most notable study was that by de la Iglesia et al.[23], who first used highly pure $Fe(DS)_3$ as an oxidant as well as a dopant-supplier to prepare PEDOT nanoparticles (not a film) via polymerization in solution. They attempted to stably disperse the polymer nanoparticles in methanol with the assistance of the dodecyl sulfate, yet the conductivity remained at the micro-Siemens level, indicating a very different purpose and result from ours. In our study, $Fe(DS)_3$ was purified very extensively by repeated washing with and recrystallization from water to ensure that the resulting PEDOT film would be of high quality and have the required reproducibility. The $Fe(DS)_3$ was then dried by using a vacuum freeze-drying method to strictly and consistently maintain its moisture content regardless of seasonal variations. Subsequently, X-ray photoelectron spectroscopy (XPS) was used to identify the atomic concentrations of the elements in $Fe(DS)_3$ (Supplementary Table 2 and Supplementary Fig. 1). In Supplementary Table 2, the 0% atomic concentration of Cl(2*p*) indicates that the Cl^- ions were completely removed to yield a highly pure iron-based surfactant.

Thermogravimetric analysis (TGA) and differential scanning calorimetry (DSC) measurements were used to study the thermal properties of $Fe(DS)_3$. The TGA curve for the oxidant sample over the range of 30–150 °C (Supplementary Fig. 2a) reveals several changes in the slope that reflect weight loss. Pereira et al.[24] studied the thermal processes of trivalent aluminum dodecyl sulfate, which is comparable to $Fe(DS)_3$ in terms of its thermal properties, and they identified a temperature region in which water loss occurred[24], which closely resembles our result. In Supplementary Fig. 2a, an analysis of Region 1, which corresponds to the first region of weight loss at 30–116 °C, provides information regarding the release of water molecules and the formation of anhydrous complexes. The curve related to the rate of mass loss displays complex trends, suggesting the existence of both occluded and bound water molecules. Based on the water loss (10.2%) measured over the temperature range 30 −126 °C, it was possible to estimate the number of water molecules present in the $Fe(DS)_3{\cdot}nH_2O$ complexes[24] as $n = 5.3$. That is, the complete formula of the compound is $Fe(DS)_3{\cdot}\mathbf{5.3}H_2O$. This formula is analogous to that of its $Al(DS)_3$

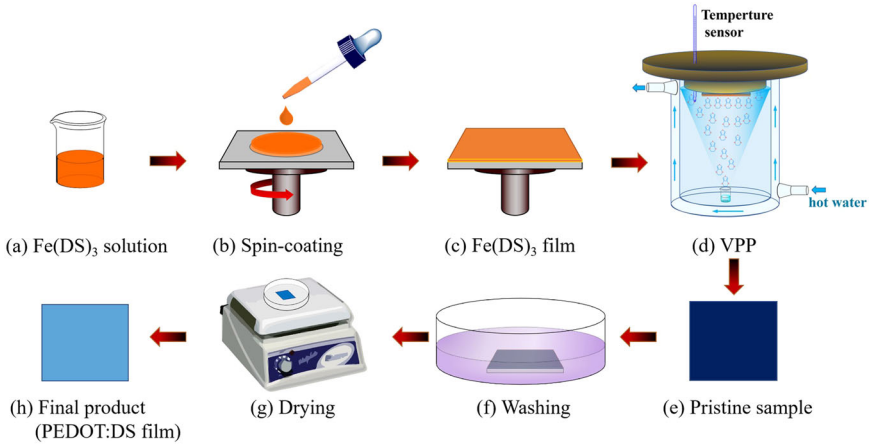

Fig. 1 | Preparation of VPP-PEDOT. Schematic representation of the preparation of the $Fe(DS)_3$ film on the substrate (**a**–**c**) and the vapor phase polymerization (VPP) process to fabricate the PEDOT:DS film (**d**–**h**).

counterpart, which is $Al(DS)_3{\cdot}4.1H_2O$. This similarity was anticipated considering that trivalent Fe and Al ions have a similar and large ability to coordinate water[25,26]. The water loss and other thermal processes of $Fe(DS)_3{\cdot}\mathbf{5.3}H_2O$ were additionally followed by means of DSC measurements (Supplementary Fig. 2b), which revealed several endothermic peaks correlated with the phase-separation of crystal water and water loss. The temperature (T_R) at which crystal water is released was identified to be approximately 48 °C as was previously determined in similar studies of $FeCl_3{\cdot}\mathbf{6}H_2O$[27,28] and the weight loss resulting from dehydration proceeds up to approximately 116 °C, in accordance with the TGA result. That is, the broad and poorly defined peak that extends from 76 °C to 116 °C corresponds to the major loss of water molecules bound in close proximity to the iron[24]. The endothermic peak at approximately 140 °C is likely to originate from the chemical transformation of $Fe(DS)_3$, a thermal process considered to start near 110 °C. Supplementary Fig. 3a shows a photograph of $Fe(DS)_3$ before and after exposure to heat at 110 °C for 10 min, during which time the color of $Fe(DS)_3$ changed from brown to black. In contrast, without heat treatment, a solution of $Fe(DS)_3$ in methanol is clear, transparent and brownish, whereas attempts to dissolve $Fe(DS)_3$ in methanol after heat treatment resulted in a cloudy suspension (Supplementary Fig. 3a). A substantial increase in the rate of weight loss at 136 °C on the TGA curve and an intense endothermic peak at 140 °C on the DSC curve clearly indicate a chemical transformation of the compound that most likely involves the hydrocarbon tails[24]. The optical microscopy image in Supplementary Fig. 3b shows a $Fe(DS)_3$ film on an oxidized Si-wafer after exposure to heat at 110 °C for 10 min. This image, indeed, does not reveal the formation of any micelles or vesicles, which indicates that $Fe(DS)_3$ underwent a complete and permanent phase transition. These coherent results strongly indicate that the $Fe(DS)_3$ molecule itself is chemically stable and intact only below 110 °C. Therefore, subsequent handling of $Fe(DS)_3$ prior to the formation of PEDOT proceeded at temperatures considerably lower than 110 °C. Apart from this, the polymerization of EDOT was not generally successful above 55 °C. As mentioned above, the water molecules bound to $Fe(DS)_3$ start undergoing phase separation at 48 °C, which indicates the release of water from the crystal phase that entails a structural change of the surfactant crystal. This suggests that the temperature and associated crystal structure of $Fe(DS)_3$ are critical for successful polymerization. Thus, by cautiously controlling the water content and temperature of the $Fe(DS)_3{\cdot}\mathbf{5.3}H_2O$ oxidant, we succeeded in preparing the most highly conductive VPP-PEDOT thin film ever reported (Fig. 1 illustrates the detailed preparation).

Table 1 | Best electrical properties of PEDOT films deposited on different substrates

Substrate	Sheet resistance (Ω sq^{-1})	Thickness (nm)	Conductivity (S cm^{-1})	Transmittance at 550 nm (%)
PET	25 ~ 44	22 ~ 42	9900 ± 200	90.8[a]
PI	30 ~ 50	20 ~ 36	9800 ± 300	90.6[b]
SiO_2-wafer	37 ~ 45	22 ~ 26	10,100 ± 400	na
ITO-coated glass*	59.1	49.7	3400	92

[a,b] From 22 nm and 24 nm thick films, respectively.
*: ITO thickness = 50 nm; sheet resistance = 60 Ω sq^{-1} on the specification sheet provided by iTASCO Corp., Korea.

Synthesis and characteristics of PEDOT:DS film

Intending to use VPP to synthesize a PEDOT film with the best possible quality, we aimed to optimize the concentration of the oxidant, polymerization time, and temperature because the thickness and quality of the film largely depend on these parameters[29,30]. The optimization is described in greater detail in the supplementary information. Table 1 summarizes the average electrical conductivities of the PEDOT films grown on PET, PI, and oxidized silicon wafer substrates, with thicknesses in the range of 20–42 nm, and corresponding sheet resistances of 50 − 25 Ω sq^{-1} with an inverse trend. Their corresponding conductivities were 9900 ± 200, 9800 ± 300, and 10,100 ± 400 S cm^{-1}, respectively, indicating that the PEDOT films were of similar quality and that their electrical properties were almost equivalent and reproducible regardless of the substrate. For comparison, the electrical properties of a ~ 50 nm-thick indium tin oxide (ITO) film are also listed in Table 1. The quality of the DS-doped PEDOT films was examined by observing the morphologies of the films synthesized on the various substrates using VPP with the aid of field effect scanning electron microscopy (FE-SEM). Immediately after synthesis *via* VPP, the pristine PEDOT films were thoroughly washed with ethanol and completely dried to obtain pure and neat films. The FE-SEM images (Fig. 2a–c) reveal that the surfaces of the PEDOT films on the oxidized Si-wafer, PI, and PET substrates, respectively, appeared clean, dense, and smooth, thereby indicating uniform growth and attesting to the nearly identical quality of the films. Of particular interest is the image in Fig. 2c, in which the film on the PET substrate is seen to have pores of a few nanometers in size and resembles a typical PEDOT polymer film. Figure 2d shows a cross-sectional image of the PEDOT film on the same substrate. The image shows that the 40-nm-thick PEDOT:DS film is very smooth and closely adheres to the substrate.

https://doi.org/10.1038/s41467-024-51621-1

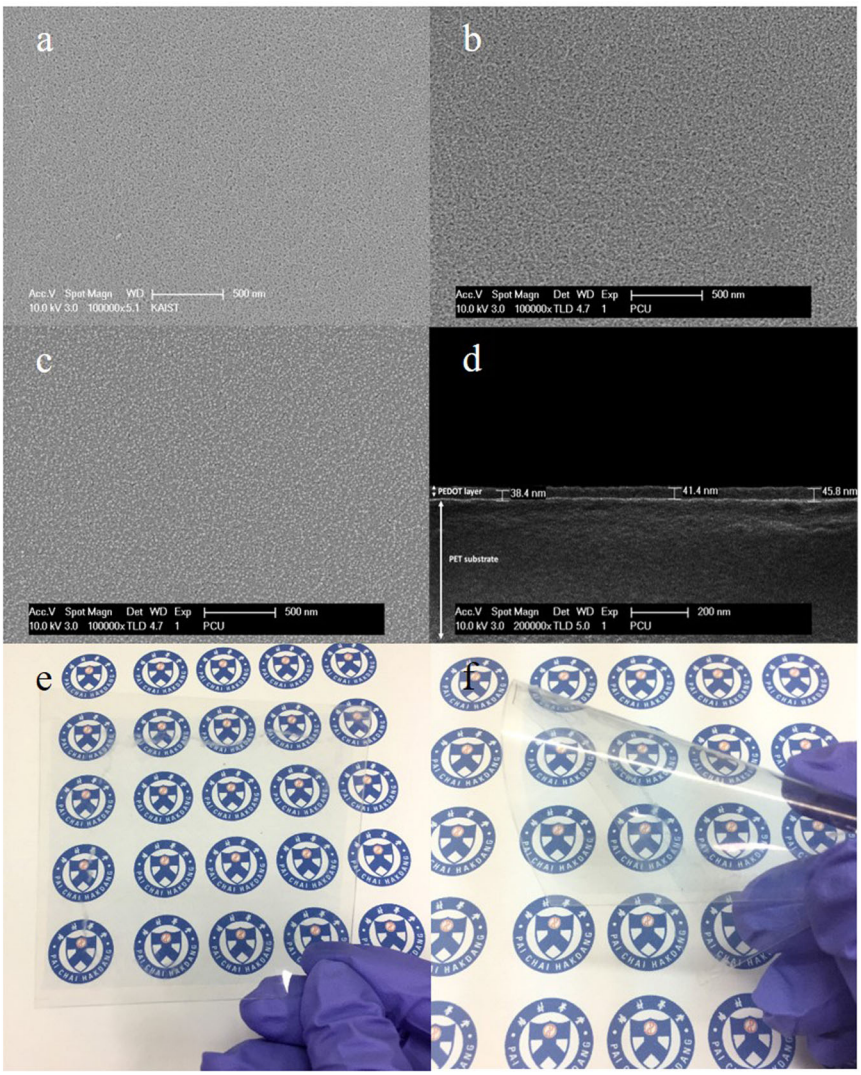

Fig. 2 | FESEM and photographic images of PEDOT:DS films. Surface morphologies of PEDOT:DS films on (**a**) SiO_2-wafer, (**b**) PI, and (**c**) PET substrates (magnification: 100k ×) (**d**) cross-sectional image of PEDOT:DS film on PET substrate. (magnification: 200k × ; film thickness ~ 40 nm) All of the films were prepared with 30 wt% $Fe(DS)_3$, and the polymerization temperature and time were 50 °C and 30 min, respectively. Photographic images of highly transparent PEDOT:DS films on PET (10 × 10 cm^2): (**e**) flat and (**f**) roll-up sheets.

The visible light transmittance and thickness of a PEDOT film are generally inversely proportional to each other, i.e., the thinner the film is, the higher the transmittance reportedly is[14,31]. The transmittance of the fabricated PEDOT:DS films was assessed by preparing these films on transparent PET substrates. Supplementary Fig. 5b shows the light transmittance at 550 nm and the conductivity as a function of the thickness of the PEDOT:DS film (refer to the visible spectrum in Supplementary Fig. 7). The transmittance and conductivity decrease with increasing thickness of the PEDOT:DS film when the thickness exceeds 25 nm. When the film is thinner than 47 nm, the corresponding transmittance is higher than 87%, which is in good agreement with previously reported results for VPP-PEDOT[14]. In fact, as an example, Fig. 2e, f show flat and roll-up images of the highly and uniformly transparent (transmittance: 91% at 550 nm) 21.1-nm-thick PEDOT:DS film on a large area of PET (size: 10 × 10 cm^2), respectively. The visible transmittance of the PEDOT:DS film on PET is therefore sufficiently high such that it would allow the conductive layer to be adopted as a transparent electrode in flexible electronics[32,33].

X-ray photoelectron spectroscopy (XPS), which was used to analyze the $Fe(DS)_3$ and PEDOT:DS films, can provide key information about the chemical composition and level of doping of a conducting polymer film[34,35]. As shown in Fig. 3a, b, the two high-resolution X-ray photoelectron bands between 166 and 172 eV represent the S 2*p* levels of the sulfur atoms in the DS moieties of the same origin, whereas the two electronic bands between 162 and 166 eV in Fig. 3b represent the S 2*p* levels of the sulfur atoms in PEDOT[17,34,35]. The S $2p_{3/2}$ and S $2p_{1/2}$ core-level spectra of the sulfates in the PEDOT film appear at 167.85 and 169.11 eV, respectively (Fig. 3b), the binding energies of which are different from those of pure $Fe(DS)_3$, which appear at 169.39 and 170.65 eV, respectively (Fig. 3a). The upward shift of the S 2*p* peaks of the DS ions in the PEDOT film relative to those of the pure oxidant originates solely from the slightly more negatively charged environment of the sulfur atoms of the dopant in the film than that of the sulfur atoms in the pure oxidant. In particular, the absence of the S 2*p* peaks of the pure oxidant from the multiplex spectrum (Fig. 3b) of the polymer film strongly indicates that the cationic sites of the thiophenes were nearly completely occupied by the dopant DS ions. The doping level of the PEDOT:DS film was calculated from the ratio of the S 2*p* peak area of thiophene to that of the dopant sulfur component[17,31,33,34]. The doping level of the PEDOT film after it was thoroughly washed with ethanol was calculated as 31.4%. This value is quite close to the previously reported theoretically maximum possible doping level (33%) of

https://doi.org/10.1038/s41467-024-51621-1

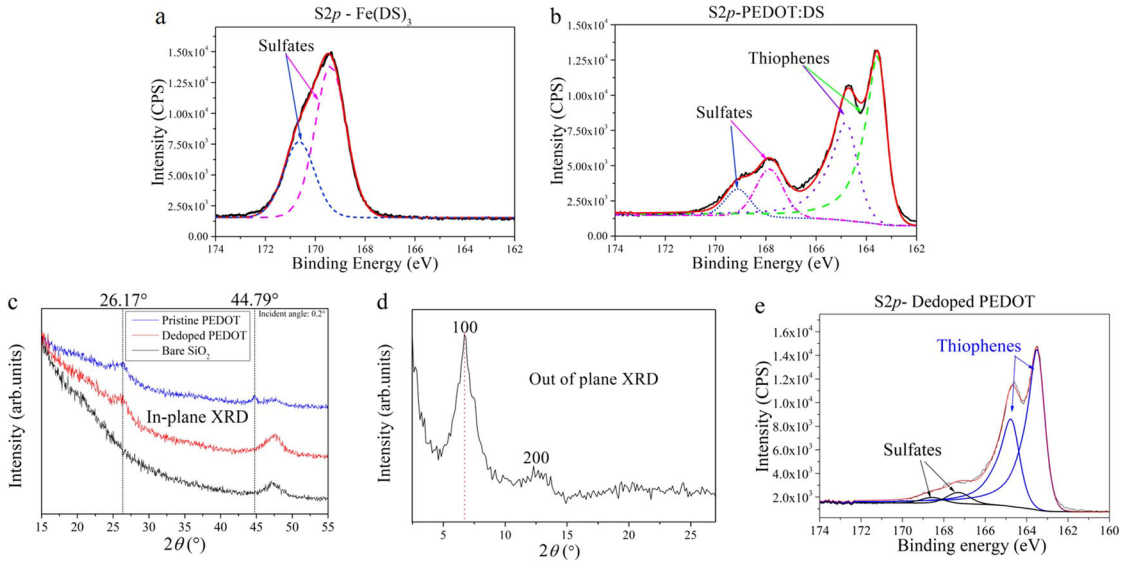

Fig. 3 | XPS and XRD spectra of Fe(DS)$_3$ and PEDOT:DS films. a, **b** S(2*p*) XPS results of Fe(DS)$_3$ and PEDOT:DS. The doublet at high binding energies (170 − 166 eV) originates from the sulfate anions and the doublet at low energies (166.5–162.5 eV) corresponds to the thiophene rings of PEDOT. **c** In-plane XRD of pristine PEDOT and de-doped PEDOT films, (**d**) out-of-plane GIWAXS diffractogram of PEDOT, and (**e**) S(2*p*) multiplex XPS of PEDOT film after de-doping.

highly conductive PEDOT films[31,33–35], suggesting that the fabricated PEDOT:DS film was nearly maximally doped with DS anions.

Crystal structure of PEDOT in PEDOT:DS film

Grazing incidence wide-angle X-ray scattering (GIWAXS) and X-ray diffraction (XRD) are powerful tools for the structural analysis of polymer thin films including PEDOT. Both in-plane XRD (incidence angle = 0.2°) and out-of-plane X-ray scattering measurements (incidence angle = 0.4°) were used to obtain a structural profile of a fully grown film. Distinct peaks were identified on the basis of previous reports[13,17,31,35,36]. The results of the XRD and GIWAXS analyses for PEDOT doped with DS ions are shown in Fig. 3c, d, respectively. The diffraction peak at 2θ = 26.17° (Fig. 3c) in the in-plane scan of XRD could be associated with the (020) diffraction peak of the PEDOT orthorhombic structure, suggesting a high degree of order in the PEDOT crystal domain. Based on Bragg's law ($2d\sin\theta = n\lambda$; $\lambda = 1.5406$ Å), the distance (d_{020}) is calculated as 3.40 Å. This value is in good agreement with the Bragg diffraction resulting from repeated π-π stacking of the adjacent PEDOT backbones, i.e., face-to-face thiophene ring stacking[13,31]. However, the intensity profile resulting from the in-plane scan of pristine PEDOT:DS exhibits two additional distinct peaks at 44.79° and 47.68°. These peaks are highly likely to originate from either DS or the substrate (oxidized Si-wafer) because any typical in-plane XRD pattern of a PEDOT crystal does not display peaks other than that at 2θ = 26.17°. To determine the origin of these peaks, the PEDOT film was de-doped with 36 wt% HCl solution by soaking the film in this solution for 30 min, followed by immersion in DI-water for 2 h. The PEDOT film was subsequently dried on a hotplate at 85 °C for 1 h, after which the in-plane XRD pattern and XPS profile were acquired. The intensities of the XPS S 2*p* peaks of the sulfates in the de-doped PEDOT at 167.65 eV and 169.13 eV are much lower than those in the pristine PEDOT (refer to Fig. 3b, e). The atomic ratios of sulfur in the DS and PEDOT, S_{DS}/S_{PEDOT}, in the pristine and de-doped PEDOT are 1/3.23 and 1/12.5, respectively, suggesting that most of the DS anions were removed during the de-doping process. Interestingly, the XRD peak at 44.79° almost disappeared after the removal of the DS dopants. This result provides clear evidence that this peak originates solely from the dopant anions, whereas that at 47.68° arises from typical diffraction pertinent to the oxidized Si substrate as confirmed by the identical peak on the XRD pattern of the bare SiO_2 substrate (Fig. 3c, black curve). On the other hand, the peak intensity at 26.17°, corresponding to the face-to-face thiophene ring stacking of PEDOT, does not change much, again indicating that the PEDOT crystal remains intact after de-doping. These coherent results from both XPS and XRD obviously support the existence of regularly ordered DS dopants and PEDOT backbones along the in-plane direction of the film. Again, based on Bragg's law, the calculated planar spacing (d_{hkl}) at 44.79° is 2.0 Å, and this periodicity is highly likely to arise from the crystalline DS vesicle in the PEDOT:DS film. This periodicity is discussed in more detail when we discuss the detailed structure of the DS vesicle in the film. Figure 3d shows the out-of-plane GIWAXS of the PEDOT film, which exhibits a sharp diffraction peak at 2θ = 6.7°, which corresponds to the typical lamellar packing of the PEDOT backbones. That is, from Bragg's equation, where the X-ray wavelength, λ, is 1.54 Å, the inter-lamellar spacing (PEDOT) is $d_{100} = 13.18$ Å. This distance is in very good agreement with previously reported values[17,31].

Crystal structure of PEDOT:DS film

Thus far, the results revealed that the structure of PEDOT in the film is a well-known typical lamellar one with repeatedly π-π overlapped polymer backbones similar to other highly conductive PEDOT films already reported except for the existence of DS crystals. The aforementioned results undoubtedly confirm that these surfactant crystals are present as dopants in the film. However, to directly observe whether the DS crystals indeed exist in the film, a high-resolution image of a PEDOT:DS film, which was partially grown on a holey carbon grid (300 mesh) for only 30 s, was successfully acquired by using Cs-corrected transmission electron microscopy (Cs-TEM) with an 80 kV e-beam. The TEM images in Fig. 4 clearly show a regularly ordered diffraction spot pattern, thereby indicating that the PEDOT:DS film is highly crystalline. However, this pattern differs considerably from that in other previously reported TEM images of PEDOT films, which show only periodicity originating from either π-π overlap or repeated lamellae of the PEDOT backbones[31,37]. This prompted us to conduct an in-depth structural study using TEM (Fig. 4), complemented by a fine molecular modeling technique and semi-empirical quantum energy calculation, to unravel the crystal structure of the PEDOT:DS film from the diffraction spot pattern. Details of this study are provided in the supplementary information and the most convincing crystal structure that was proposed is depicted in Supplementary Figs. 24b and 26.

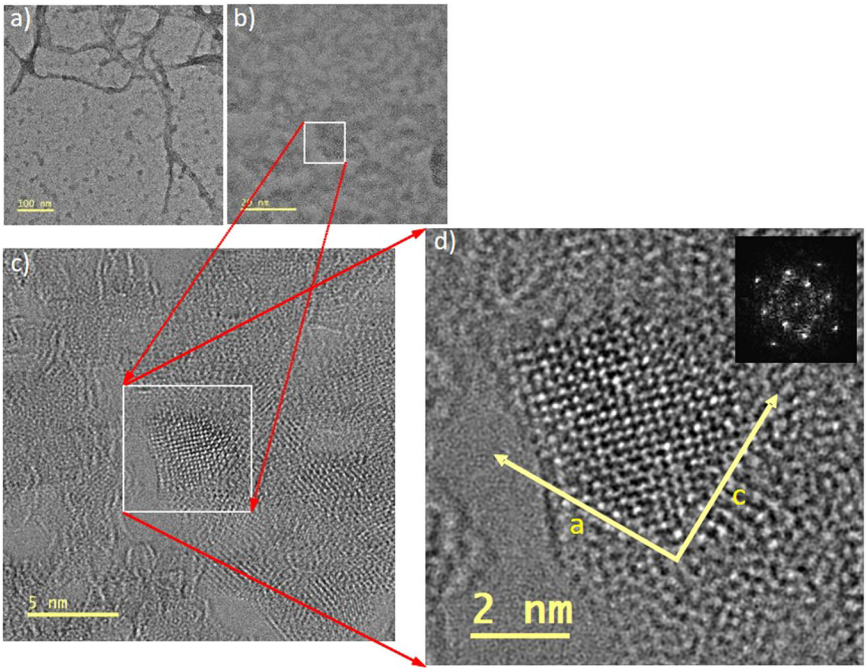

Fig. 4 | Cs-HRTEM images of PEDOT:DS crystal. Electron micrograph images at an early stage (after 30 s) of polymerization of a PEDOT:DS crystal grown on a holey carbon grid. The images were taken at (**a**) 50k ×, (**b**) 400k ×, and (**c**) 1.5 M × magnification, respectively. The a- and c-axes in the image in (**d**) denote the orientation of the PEDOT crystal. The image in the inset in (**d**) is a fast Fourier transform (FFT) of the TEM image of the PEDOT:DS crystal. The residual astigmatism in (**c**) and (**d**) is a phenomenon that is commonly observed in an ultra-thin layer grown on a holey carbon grid[38].

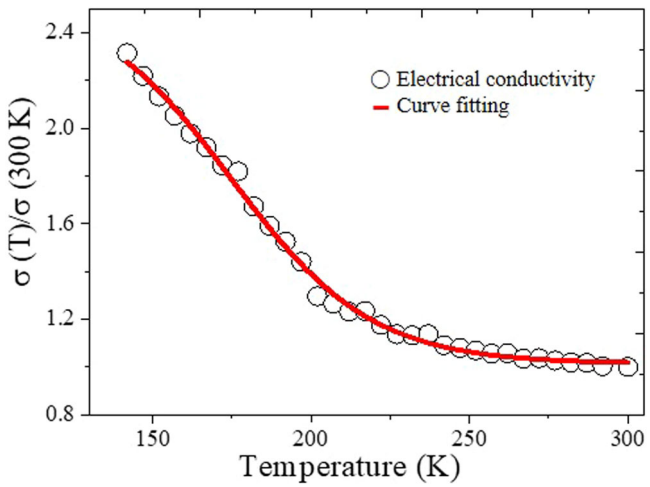

Fig. 5 | Temperature dependence of conductivity. Electrical conductivity was normalized at 300 K.

The overall crystal structure of the PEDOT:DS film proposed in the supplementary information suggests important implications, i.e., that the repeating lamellar superstructures of the $Fe(DS)_3$ MLV proposed in Supplementary Fig. 17 guide the growth of stacked PEDOT crystalline domains. Indeed, the structure of the dopant crystal in the polymer film is nearly identical to that of the oxidant crystal. Consequently, based on the proposed crystal structure of the PEDOT:DS film, it is appropriate to imagine ways in which EDOT monomers could start to be oxidized and polymerized on the Fe^{3+} ion-rich layers of the DS lamellae. These sufficiently spacious lamellae (which form a lamellar superstructure) would allow easy access to the EDOT monomers at the beginning stage of VPP to enable the growth of large PEDOT crystalline domains. Once the polymer crystal starts growing, the EDOT monomers could enter and grow through the space between the upper and lower DS monolayer planes. This would probably be driven by a strong hydrophobic attraction between the hydrogen atoms of the polymer and DS chains along the diagonal direction orientated 41° to the axis of the dodecyl chain, as designated by the red arrows in Supplementary Figs. 17c-iii and 26. During the growth, it is reasonable to consider that reduced Fe^{2+} ions and solvent molecules are ejected from the inter-lamellar space probably because the growing PEDOT crystal is increasingly occupying this space. As a result, the superstructure could be expected to gradually collapse, with its two opposing polar head groups eventually approaching each other to intimately interface for doping. It is also reasonable to imagine that EDOT monomers enter the inter-space between two DS monolayer planes in the laterally tilted (45.5°) or completely flat orientation because the average height of the inter-space (~ 2.5 Å) shown in Supplementary Fig. 17c–i is insufficient to accommodate these monomers in the vertical orientation (~ 4.8 Å). However, more precise structural dimensions and a more detailed growth mechanism of the PEDOT:DS co-crystal in the un-contracted state (Refer to Supplementary Fig. 24) would have to be determined. In addition, more specific information about the crystalline phase change, particularly during film growth would be required. A more meticulous study is currently underway.

Additional support for the highly crystalline structure of the PEDOT:DS film could be provided by the temperature dependence of its conductivity, which was promptly measured, as shown in Fig. 5. The graph shows the change in the slope of the σ-vs.-T plot for the temperature range 300–140 K. The electrical conductivity (σ) increases sharply as the temperature decreases downward from room temperature. This behavior is typical of a pure metallic material because the more crystalline or metallic the polymer film is, the more conductive it tends to become as the temperature decreases[9]. In other words, the slope of σ vs. T is negative and changes considerably faster than that previously reported for highly conductive and crystalline PEDOT films[9]. For example, the negative slope of the σ-vs.-T plot, particularly for the temperature range 225–140 K, changes nearly 17 times faster than that of the PEDOT:Tosylate film mixed with PEG-PPG-

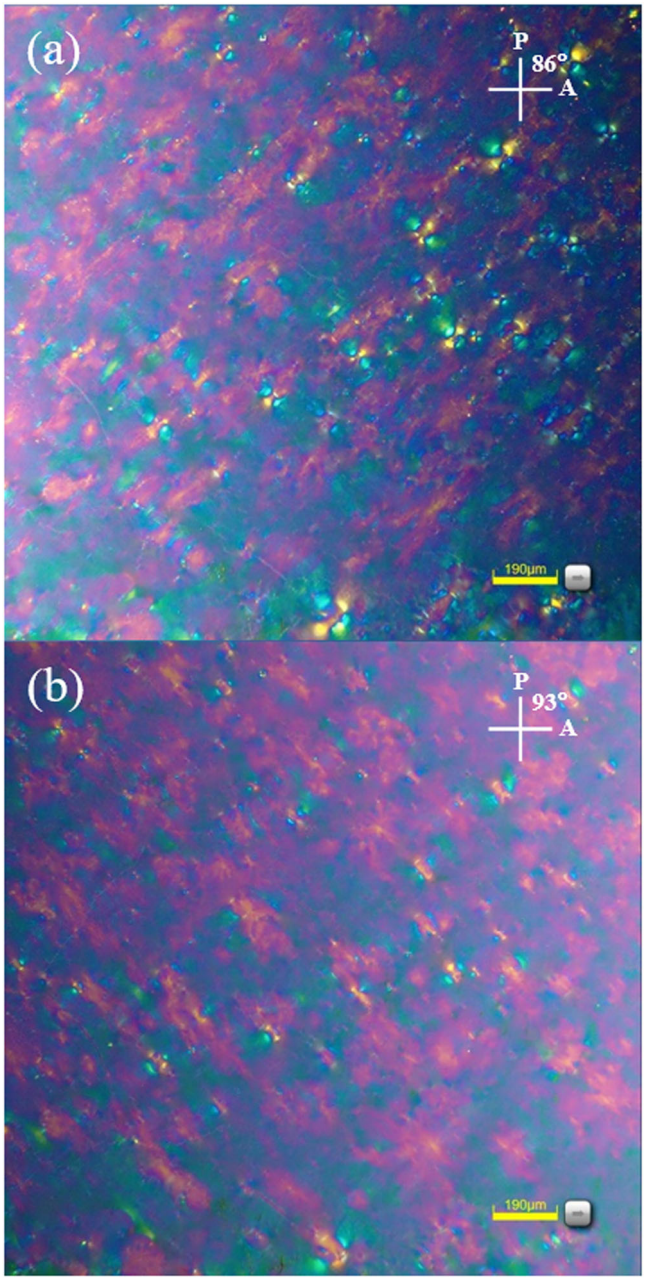

Fig. 6 | Polarized light microscopy images of PEDOT crystal domains (reddish color). Right- (**a**) and left-tilted (**b**) growth of PEDOT crystal domains. Magnification: 145 ×; substrate: SiO_2 wafer; film thickness = 32 nm; Scale bar = 190 μm.

PEG (5800 M_w) and dimethylformamide (DMF) as additives over the same temperature range[9]. In some other cases, the slope even follows the completely opposite trend[38], suggesting that charge transport occurs largely by way of a hopping mechanism. This indicates that the crystal domains of the PEDOT:DS film are very large. In fact, the polarized light microscope images shown in Fig. 6 and Supplementary Fig. 27 reveal that the PEDOT crystal domains (reddish color) are enormous and that they grew along two different intercrossing directions as shown in Fig. 6a, b. In addition, the images in Supplementary Fig. 27c–f clearly show the existence of dodecyl sulfate lamellar crystals, which have blue Maltese cross-like interference patterns, as shown in Supplementary Fig. 16. This directional growth of the PEDOT crystal domains as a result of the presence of the dodecyl sulfate lamellar crystals further supports that the PEDOT crystal indeed grows through (i.e., penetrates) the lamellar superstructure of the oxidant vesicles. These polarized light images also fully explain why the PEDOT particles, polymerized with $Fe(DS)_3$ in solution, as reported by de la Iglesia et al.[23], are nanometer-sized and have very low conductivity. This is because the formation of a large-sized lamellar superstructure is very difficult, particularly when the oxidant is in the solution phase and completely dissolved in methanol; in other words, the superstructure only forms in the highly concentrated state such as when spin coating during VPP. Moreover, as shown in the images, these two intercrossing crystal domains nearly extend across the entire film and are firmly indicative of the predominance of domain-to-domain charge transport in the polycrystalline film. This uniformly entangled and ultra-large polycrystalline phase that covers the entire PEDOT:DS film well explains the superb electrical conductivity (~ 1.0×10^4 S cm^{-1}) of the film. Nevertheless, this film, which is sensitive to polarized light, is obviously completely anisotropic, and thus the macroscopic orientation of the polycrystalline domains is quite random, even though the domains are highly ordered at the nanometer scale. This is strongly ascertained by the fractal tree-like pattern of the crystal as shown in Fig. 6 and Supplementary Fig. 27. The lack of long-range ordering in the film is further supported by the in-plane XRD pattern of the $Fe(DS)_3$ vesicles in Supplementary Fig. 15. The appearance of all three possible major diffraction peaks in the same in-plane geometry of the lamellar crystal (Supplementary Fig. 15) strongly suggests that the crystal domains are randomly oriented, which means that the PEDOT film was rendered highly anisotropic as a result of VPP. This result also well explains why both the in-plane and out-of-plane XRD patterns in Fig. 3c, d show slightly less intense and less well-resolved peaks than the relatively highly ordered PEDOT despite the very large expanse of the PEDOT:DS polycrystalline domains.

Mechanical property of PEDOT:DS film

The mechanical flexibility and durability, which are essential figures-of-merit for an FTE, of pure and highly conductive PEDOT thin films doped with any molecules except the PSS anion are commonly inferior as compared to competing materials such as graphene. This is mainly attributed to their high brittleness[39,40]. We therefore considered it important to evaluate whether the use of $Fe(DS)_3$ as an oxidant as well as a dopant-supplier actually improves the mechanical flexibility and durability of the PEDOT:DS film. The evaluation consisted of a series of mechanical tests. Specifically, the films polymerized on PET and PDMS, respectively, were subjected to bending and stretching tests to monitor the resistance changes to assess the flexibility and durability of the film. The variation in resistance can be expressed as $\Delta R = (R - R_0)/R_0$, where R_0 is the initial value of the resistance, and R is the resistance measured by using the two-point probe method (see Fig. 7a) either during bending or immediately after a certain number of cycles of successive bending. Figure 7b shows the variation in R as the radius of curvature of a PEDOT film on a PET substrate decreases. As shown, the resistance of the film is nearly constant until the bending radius reaches 0 mm. The resistance ($\Delta R/R_0 = 7\%$) was detected to increase slightly only for complete folding (0 mm radius of curvature) such as for origami, as seen in Fig. 7b. Figure 7c shows the results of a dynamic bending fatigue test carried out with the PEDOT:DS film grown on PET. The film was repeatedly bent in either the inner or outer directions for as many as a million cycles with a bending radius of 1 mm and frequency of 2 Hz (see Fig. 7c and the movie file). The test revealed nearly no change in resistance up to 5×10^5 inner and 2×10^5 outer bending cycles. Even at the maximum of 1×10^6 bending cycles, the resistance of the film increased by only 2% and 12% for inner and outer bending, respectively. The larger increase in the resistance for outer bending reflects the greater susceptibility of the polymer film to tension than to compression, as would generally be expected[41]. The stretchability was tested by preparing a PEDOT:DS film on PDMS (Fig. 8a). The film, which has a sheet resistance of 38.9 Ω sq^{-1} and a thickness of 45 nm, was stretched out along the direction of the PDMS

https://doi.org/10.1038/s41467-024-51621-1

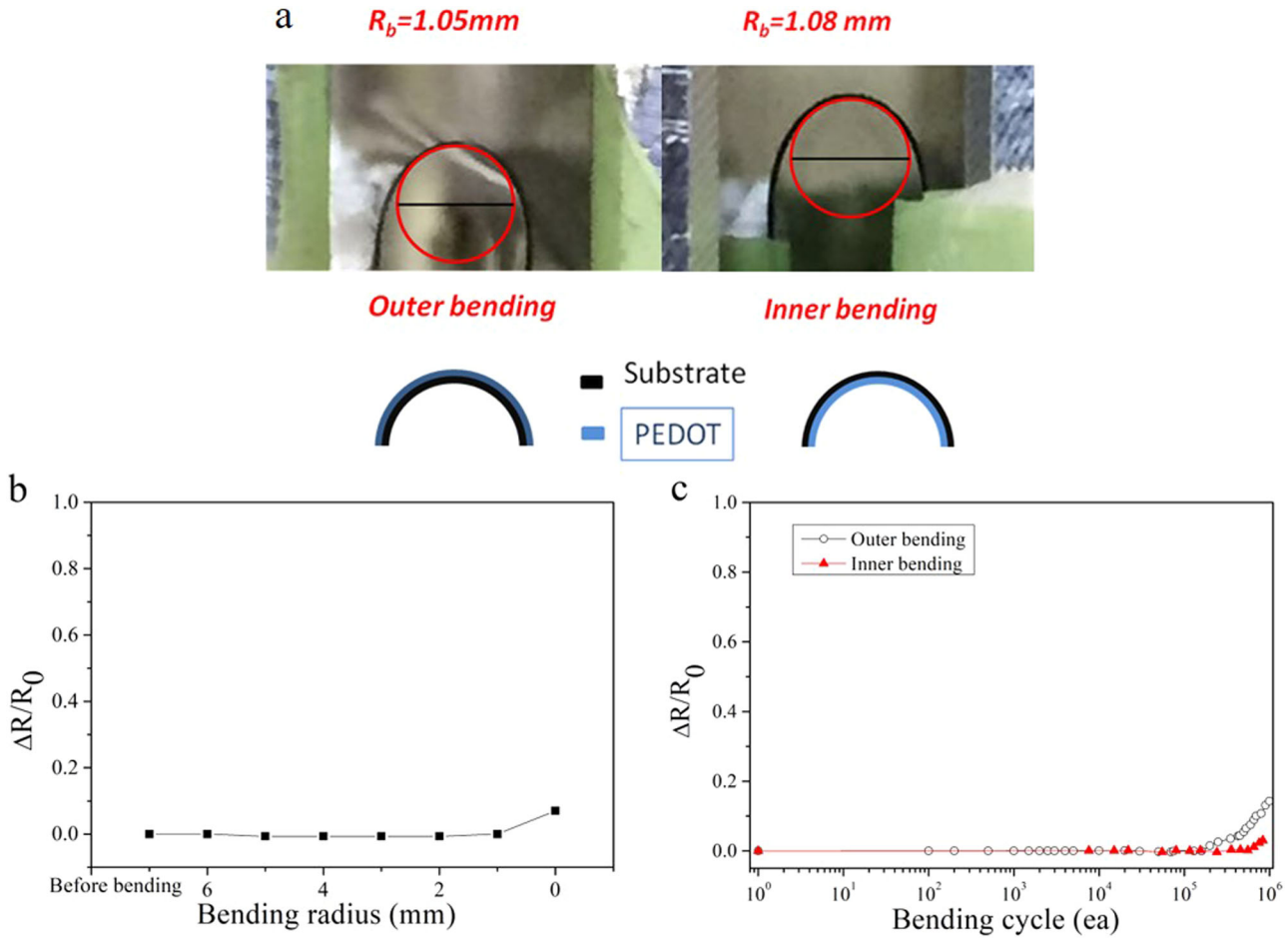

Fig. 7 | Mechanical durability test of PEDOT/PET film. a Photographs of the PEDOT/PET film bent to the maximum outer and inner bending radii. Variation in the resistance of the PEDOT/PET film with (**b**) increasing bending radius and (**c**) increasing bending cycles. Outer and inner bending are denoted by the open circle and red triangle, respectively.

substrate. The variation in the resistance of the film with increasing strain during a dynamic stretch test of the polymer film is plotted in Fig. 8b. The variations in the resistance of the film were fairly minor at 3% and 10% for 20% and 30% tensile strain, respectively (the PEDOT/PDMS film was fixed between two glass holders and elongated from 20 mm to 26 mm to reach 30% tensile strain). In addition, for up to 30% stretching, the resistance values were completely reversible, which means that the film was not damaged by stretching at all and quickly recovered from the strain.

The slight change in resistance up to 5×10^5 inner- and 2×10^5 outer-bending cycles indeed demonstrates that the densely packed crystal monolayer of DS dopant molecules that cover nearly all of the intersectionally grown PEDOT polycrystals, as shown in Fig. 6 and Supplementary Fig. 27, dramatically improves the mechanical durability and flexibility of the film. This impressive mechanical strength and high flexibility of the PEDOT:DS film is incomparable with those of any of the other highly conductive pure polymer films ever reported[42–44]. In addition, the minor increases in resistance upon complete folding ($\Delta R/R_0 = 7\%$) and stretching up to 20% tensile strain ($\Delta R/R_0 = 3\%$) further prove the greatly improved flexibility as well as mechanical durability of the film. The static bending and stretching properties of the film fabricated in this study are fairly close to those of a film consisting of a graphene monolayer[45,46]. Equally noteworthy is that the cyclic bending property of the PEDOT:DS film developed in this study is far superior to that of a polycrystalline graphene film ($\Delta R/R_0 \geq 10\%$ of a three-layered graphene film for 2000 bending cycles and a rate of 2.0 Hz, respectively)[47]. These superior mechanical properties of the PEDOT:DS film obviously reflect that it is more durable and flexible than a graphene film at least at the micrometer scale or larger. Apart from this, numerous studies have demonstrated polymeric film with distinctly improved mechanical durability and flexibility with the aid of surfactants with long hydrocarbon tails, such as sodium dodecyl sulfate (SDS) and sodium dodecylbenzenesulfonate, to name but a few[48–50]. These surfactants were definitely shown to play a core role in noticeably improving the durability and flexibility of polymeric films. For instance, Wang et al.[48] reported a PEDOT:PSS thin film that contains various ionic surfactants to enhance the electrical conductivity and mechanical strength at the same time. This film maintained fairly high electrical conductivity (4100 S cm^{-1}) even at 100% tensile strain. The authors attributed the dramatically improved durability and stretchability at least partly to surfactant-type additives with long hydrocarbon tails, which serve as both conductivity and stretchability enhancers at the same time.

Stability of PEDOT:DS film in water

Water resistance is considered to be an important parameter for the evaluation of a conductive polymer film for use as an electrode under wet conditions such as in a flexible battery or supercapacitor[51]. The PEDOT:DS film was exposed to deionized water for 30 days to test the water resistance of the film. The two-point probe method was used to monitor the variation in the resistance of the PEDOT film, and the film was dried overnight in a desiccator before every measurement. The initial resistance of the film was $43.1 \pm 5.3\ \Omega\ sq^{-1}$. The variation in the sheet resistance of the film immersed in water is plotted in Fig. 8c.

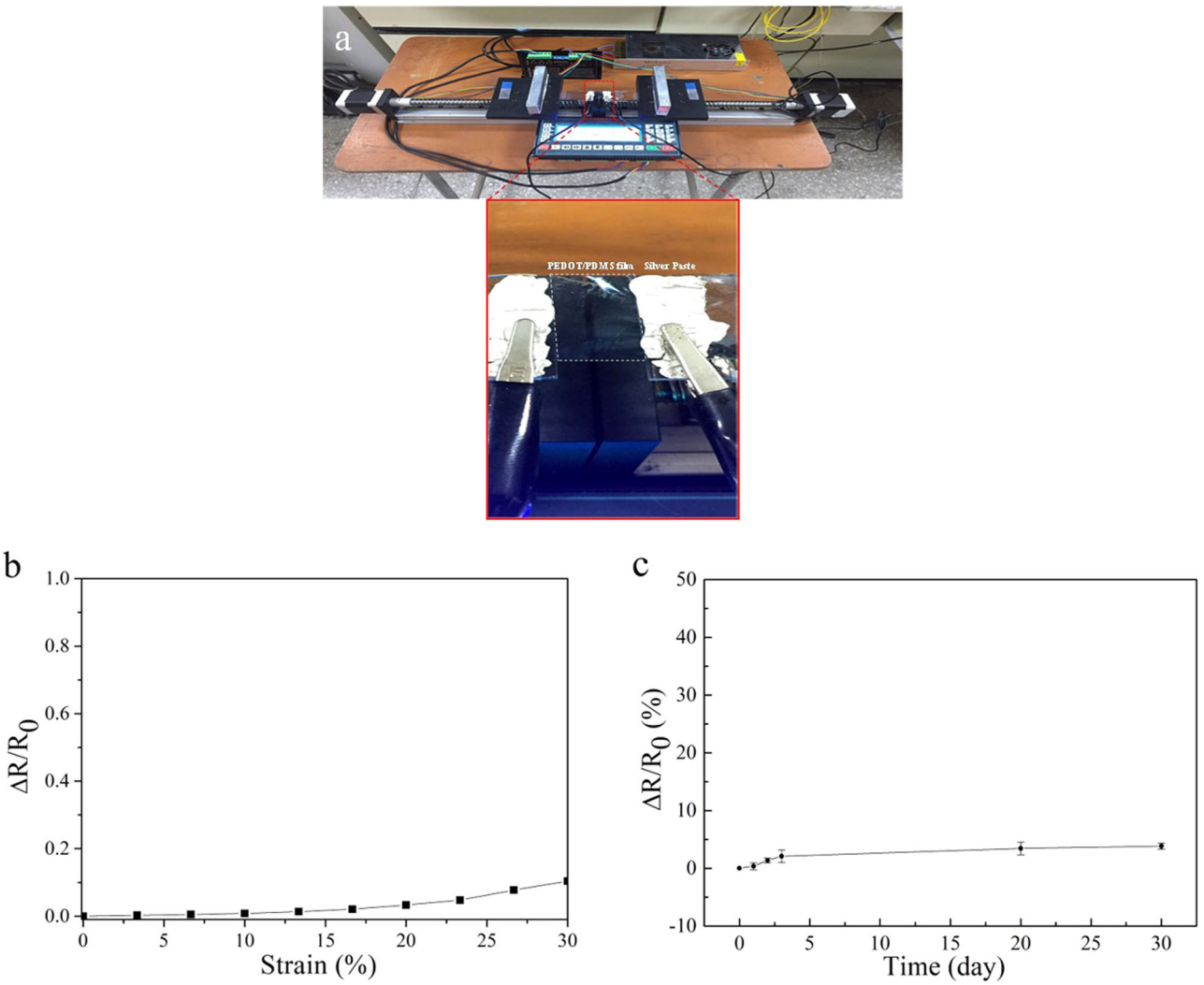

Fig. 8 | Stretchability and water-stability test of PEDOT:DS film. a Photograph of a stretched PEDOT film on a PDMS substrate (size: 30 mm × 25 mm; t = 0.5 mm) at 30% tensile strain. **b** Variation in the resistance of the PEDOT:DS film with increasing strain. **c** Variation in the sheet resistance of a PEDOT film on PET versus the number of days of immersion in water at room temperature. Variations in the resistance are 0.4 ± 0.6 (1 day), 1.4 ± 0.4 (2 days), 2.1 ± 1.1 (3 days), 3.4 ± 1.1 (20 days), 3.8 ± 0.5 (30 days), respectively.

After 30 days, the sheet resistance increases from the initial 43.1 Ω sq^{-1} to 44.7 Ω sq^{-1} (an increase of only 3.8%), indicating excellent water resistance. This result compares very favorably with that obtained by Ala et al.[52], who tested the water stability of a PEDOT film that was vapor phase-polymerized on a cotton fiber. They reported a large increase in the sheet resistance from ~ 60 Ω sq^{-1} to ~ 500 Ω sq^{-1} even after only 2500 min (1.7 days), mainly because water molecules could easily penetrate the film. Accordingly, the stability of the PEDOT:DS film mainly originates from the hydrophobic alkyl chains of the DS vesicles that tightly and nearly completely surround the PEDOT crystals, thereby effectively preventing the penetration of water molecules into the film from interfacing aqueous media. Additional support for this finding is that the static water contact angle of the PEDOT film measured in this study is 71°, as shown in Supplementary Fig. 28. This angle indicates that the film is much more hydrophobic than other previously reported tosylate-doped VPP-PEDOT films with a static water contact angle of 44°[53] or are even completely hydrophilic[35]. A DS-doped PEDOT conductor with excellent water stability could be an indispensable component of any flexible electronic device, e.g., a skin-attachable or implantable biosensor, where it would have to operate for long periods of time during exposure to humid or aqueous media[54].

Our study indicated that the MLVs of iron(III) dodecyl sulfate ($Fe(DS)_3$), a key factor for the VPP of EDOT at a different level, delicately direct the growth of a highly conductive, transparent, and durable but still highly flexible film. This simple one-step process is possible without the aid of any additive or additional dopant, which means it is cost-effective. The important findings of this study are summarized as follows. The exact chemical formula of the iron(III) dodecyl sulfate used in this study was determined to be $Fe(DS)_3$·**5.3**H_2O. The electrical conductivity of the DS-doped PEDOT film reaches an average of ~ 1.0×10^4 S cm^{-1} (the thickness and transmittance of the film were 21 nm and ~ 90% at 550 nm, respectively.). In particular, the conductivities of the PEDOT films on various substrates are nearly identical. The structural study strongly suggested that intersectionally grown polycrystals of PEDOT lamellae consist of repeated layers of densely packed polymer backbones interspersed with dodecyl sulfate crystal monolayers and DS dopant molecules. The PEDOT:DS film grown on PET had truly exceptional mechanical durability, flexibility, and water resistance. After 500,000 inner- and 200,000 outer- bending cycles of the film, $\Delta R/R_0 \approx 0\%$ for a bending radius of 1 mm and at a rate of 2 Hz, respectively. After immersion in an aqueous medium for one month, the PEDOT film was still intact with almost no increase in the resistance. These favorable properties of the

VPP-PEDOT film mainly originate from the directional growth of the polymer crystal in the lamellar superstructures of the $Fe(DS)_3$ film, which formed particularly in the highly concentrated state. During VPP, the superstructure DS-MLVs have several concurrent functions – a most effective oxidant without side reactions, a highly efficient in situ dopant, a template to facilitate the large-scale growth of polycrystalline domains, and an enhancer of the water resistance and durability. We anticipate these unique and important findings to provide new directions and insight into the synthesis of more conductive, transparent, robust, water-resistant, and flexible but cost-effective polymer electrode materials by guiding the development of MLVs with more adjustable size and structure for a surfactant-type oxidant in future.

Methods

Materials

The monomer, 3,4-ethylenedioxythiophene (EDOT), methanol, ethanol, iron(III) chloride, sodium dodecyl sulfate (SDS), and sodium 1-octadecyl sulfate were purchased from Sigma-Aldrich, USA. Sodium n-octanoate, sodium mono-octyl phosphonate, sodium mono-octyl phosphate, and sodium mono-dodecyl phosphate were purchased from TCI, Japan. Sodium 1-dodecane sulfonate was purchased from Alfa Aesar, USA. Ultra-pure water (18 MΩ·cm), purified with a water purification system from Barnstead, USA, was consistently used throughout this study. All materials were used as received without further purification. The Sylgard 184 silicone elastomer kit for PDMS was purchased from Dow Silicone, USA. Polyethylene terephthalate (PET) and polyimide (PI) of the highest quality were purchased from Koron Industries and SK Industries in Korea, respectively. The SiO_2-wafer was purchased from University Wafer Inc., USA. The ITO-coated glass (ITO thickness = 50 nm; Rsq = 60 Ω/□) was purchased from iTASCO, Korea.

Preparation of iron(III) dodecyl sulfate ($Fe(DS)_3$)

A solution of sodium dodecyl sulfate (SDS, 10.25 g, 0.148 mol/L) in deionized (DI) water was prepared by adding the SDS to water followed by heating and stirring at 40 °C until the solution became transparent. To this solution, an aqueous solution of $FeCl_3$ (0.197 mol/L) was slowly added while stirring (molar ratio of SDS to $FeCl_3$ = 3:1). The precipitate was washed repeatedly with DI water at least 10 times and subsequently dissolved in 45 mL methanol and centrifuged at 5394 × *g* to remove insoluble impurities (Labogene 1248, Korea). The methanol solution was transferred to a 500 mL beaker, to which 200 mL DI water was added very slowly while stirring, whereupon a large amount of $Fe(DS)_3$ precipitated from the solution. The recrystallized $Fe(DS)_3$ was repeatedly washed at least five times. The purified $Fe(DS)_3$ was freeze-dried for at least 2 days (FDU 1200 freeze dryer, Eyela, Japan). All the other iron(III) surfactants were prepared using the same procedure as for $Fe(DS)_3$.

Preparation of PEDOT films

The detailed procedure is illustrated in Fig. 1.

Preparation of oxidant ($Fe(DS)_3$) film.

(1) The thermally oxidized-Si wafer (University Wafer Inc., 200 nm SiO_2 layer, 1.5 cm × 1.5 cm), PET, PI, and PDMS substrates (1.5 cm × 1.5 cm or 10 cm × 10 cm) were cleaned in an ethanol bath using ultrasonication (Branson 3510-DTH, USA) for 30 min and used without further cleaning. Then, a solution of the oxidant (10 – 60 wt.%) was dropped on the substrate and left for at least 3 min prior to spin-casting at 1500 rpm for 20 s (JSP 4D, JD Tech, Korea), after which a certain amount of the solvent in the spin-coated film must be uniformly distributed on the substrate to ensure the uniform growth of PEDOT.

Vapor phase polymerization (VPP) of EDOT to form the PEDOT films.

(2) The oxidant-coated substrate was transferred into a reaction chamber with a volume of 3.0 L (Fig. 1), to which 0.5 mL EDOT (cup diameter = 13 mm; height = 10 mm) and 0.5 mL water (cup diameter = 26 mm; height = 10 mm) were added beforehand. The distance between the substrate and source inside the chamber was always maintained at 200 mm. The chamber temperature was controlled by a hot water jacket built into the wall of the chamber and was monitored using a temperature sensor that extended into the chamber such that it was positioned at the level of the substrate inside the chamber (see Fig. 1). After polymerization (< 30 min), the samples were extensively washed with ethanol to remove surplus oxidant and EDOT monomers that remained on the PEDOT film. Finally, the washed PEDOT film was dried at 85 °C for 1 h to remove the ethanol.

Characterization

The thermal stability of $Fe(DS)_3$ was assessed with differential scanning calorimetry (DSC) and thermogravimetric analysis (TGA) (Mettler-Toledo, 1600 LF, USA). The $Fe(DS)_3$ was freeze-dried for 2 days before the thermal analyses (Sample weight: 5.4 mg for DSC and 6.85 mg for TGA; heating rate: 10 °C/min for both analyses). Field emission scanning electron microscopy (FE-SEM) (Sirion, Netherlands) was used to characterize the topography and morphology of the PEDOT film. The film was grown on a SiO_2-wafer or PET substrate and then freeze-dried for 1 day before analysis. Before imaging, a 10-nm-thick Pt layer was coated on the sample surface by sputtering (e-beam energy: 10 – 15 kV; spot size: 3.0 nm). Microscope images of all the materials were captured with Olympus microscopes (DSX1000 and BX51), Japan. The sheet resistance (R_{sq}) of the PEDOT film was measured with a four-point probe (Keithley 2182 A nanovoltmeter and 2400 source/meter, USA). In some cases, a two-point probe measurement was carried out with an HP4155A semiconductor analyzer and a probe station (MS-Tech, Korea). The electrical conductivity (σ) of the thin film is defined as

$$\sigma = \frac{1}{R_{sq}t} \tag{1}$$

where R_{sq} is the sheet resistance and t is the thickness of the PEDOT:DS film, which is obtained from the FE-SEM image. The tip of the four-probe head of the four-point-probe stage has a diameter of 100 µm. The distance between two neighboring tips is 1 mm. The resistance is calculated by *V*/*I*, where *V* and *I* can be measured with a voltmeter and current source, respectively. In this case, the sheet resistance was calculated as:

$$R_{sq} = \frac{\pi}{\ln(2)}\frac{V}{I} = 4.532\frac{V}{I} = 4.532R \tag{2}$$

For example, for a 21-nm-thick PEDOT:DS film on the PET substrate, R_{sq} = 4.532*R = 4.532*10.19 Ω/sq = 46.2 Ω/sq, where 10.19 Ω is calculated from *V*/*I*. Therefore, the conductivity must be:

$$\sigma = \frac{1}{R_{sq}t} = \frac{1}{46.2 \times 21 \times 10^{-7}}(\Omega \cdot \mathrm{cm})^{-1} = 10307(S/cm) \tag{3}$$

The XPS surface analysis was performed with K-α+ equipment at Busan Center, Korea Basic Science Institute, manufactured by ThermoFisher Scientific, USA (energy resolution ≤ 0.5 eV FWHM; sensitivity for narrow scan: 1MCPS @ 0.6 eV or higher; Beam size: 200 µm; detection depth: 10 nm). $Fe(DS)_3$ and PEDOT films were prepared on SiO_2-wafer substrates and then freeze-dried for 1 day before analysis. Visible (UV-2450, Shimadzu, Japan) and Raman (FEX, NOST, Korea)

spectra of the PEDOT:DS films were recorded to examine the transparency and polymerization, respectively. Grazing incidence X-ray diffraction measurements were acquired with synchrotron radiation (Postech, Korea) using a 3D – X-ray scattering beamline (beam size: 0.5 × 1.0 mm^2; beam energy: 6 – 12 keV; incidence angle: 0.4°) for an out-of-plane scan. In-plane XRD scans were acquired with a SmartLab X-ray generator with a 9 kW rotating anode and Cu tube at KITS with an incidence angle of 0.2° (θ-θ vertical type scan; goniometer radius: 300 mm; minimum step: 0.0001°) for the PEDOT:DS film, and a 9 kW rotating anode and Cu tube with an incidence angle of 0.3° (θ-θ vertical type scan; goniometer radius: 300 mm; minimum step: 0.08°) for the $Fe(DS)_3$ film. Spherical aberration corrected (Cs)-high resolution transmission electron microscope (Cs-HRTEM) images were taken using a JEM ARM-200F with Cold FEG (Image Cs-corrector, JEOL, JAPAN) at 80 kV. The Cs-HRTEM images were captured with a sensitive CMOS camera (OneView camera, GATAN, US; 25 fps at full 4k × 4k resolution), enabling atomic scale details to be studied by very low-dose and high contrast imaging for beam-sensitive materials and elements (low atomic number). To minimize electron beam damage, Cs-HRTEM investigations of the PEDOT:DS film were carried out using low doses equal to approximately 280 electrons/$Å^2$. This dose was calculated from the measurement (~0.2 pA/$Å^2$) of a Faraday cup in the absence of the specimen. Visual inspection of the magnified images did not reveal any changes in the image detail that could have arisen from electron beam damage. The filtered images presented in this paper were reconstructed using a Fourier diffractogram of the original image and with an aperture surrounding the diffraction spots in the diffractogram (low-pass spatial filtering) to remove noise originating from the scan and counting statistics from the original image. All energy calculations were performed with the Gaussian 16 package. The rigid energy scan over the central axis of the carbon atoms in the dodecyl group was carried out using the semi-empirical AM1 method in 36 steps with 10° increments (0° to 360°) to determine the lateral tilting angle of the DS chain. Molecular modeling was accomplished using ChemDraw Professional 16.0 and Chem3D 16.0. Low-temperature measurements of the film conductivity were carried out as follows. The PEDOT:DS film was inserted into a stone holder, whereupon the four-point probe and temperature sensor were attached to the sample surface. The holder, including the sample, temperature sensor, and four-point probe, was placed in a small vacuum-sealed chamber, and then the chamber was placed under a vacuum. The chamber was completely surrounded by liquid nitrogen and left to reach 140 K for the resistance measurement. Subsequently, the chamber was removed from the liquid nitrogen very slowly to record the corresponding resistance values at temperatures higher than 140 K. The static water contact angle of the PEDOT:DS film was measured with a contact angle analyzer (Phoenix 150, Surface Electro-Optics, Korea) by using the sessile drop method. Bending and stretching tests were carried out with equipment from Bo Chao Transmission Equipment Co. Ltd., China.

Data availability

Most of the data presented in this study have been deposited in the figshare database [https://doi.org/10.6084/m9.figshare.25816438]. All other data are available from the corresponding author upon request.

References

1. Ouyang, J. Application of intrinsically conducting polymers in flexible electronics. *SmartMat* **2**, 263–285 (2021).
2. Kim, Y., Kim, Y. & Kim, J. H. Highly conductive PEDOT:PSS thin films with two-dimensional lamellar stacked multi-layers. *Nanomaterials* **10**, 2211–2221 (2020).
3. Cui, H. et al. Optimization of ethylene glycol doped PEDOT:PSS transparent electrodes for flexible organic solar cells by drop-casting method. *Chinese J. Polym. Sci.* **37**, 760–766 (2019).
4. Chou, T., Chen, S., Chiang, Y., Lin, Y. & Chao, C. Highly conductive PEDOT:PSS films by post-treatment with dimethyl sulfoxide for ITO-free liquid crystal display. *J. Mater. Chem. C* **3**, 3760–3766 (2015).
5. Song, J. et al. High-conductivity, flexible and transparent PEDOT:PSS electrodes for high performance semi-transparent supercapacitors. *Polymers* **12**, 450–460 (2020).
6. Shi, Y., Zhou, Y., Shen, R., Liu, F. & Zhou, Y. Solution-based synthesis of PEDOT:PSS films with electrical conductivity over 6300 S/cm. *J. Ind. Eng. Chem.* **101**, 414–422 (2021).
7. Yeon, C., Yun, S. J., Kim, J. & Lim, J. W. PEDOT:PSS films with greatly enhanced conductivity via nitric acid treatment at room temperature and their application as Pt/TCO-free counter electrodes in dye-sensitized solar cells. *Adv. Electron. Mater.* **1**, 1500121 (2015).
8. Schultheiss, A. et al. Insight into the degradation mechanisms of highly conductive poly(3,4-ethylenedioxythiophene) thin films. *ACS Appl. Polym. Mater.* **2**, 2686–2695 (2020).
9. Gueye, M. N., Carella, A., Faure-Vincent, J., Demadrille, R. & Simonato, J. Progress in understanding structure and transport properties of PEDOT-based materials: A critical review. *Prog. Mater. Sci.* **108**, 100616 (2020).
10. Bubnova, O. et al. Semi-metallic polymers. *Nat. Mater.* **13**, 190–194 (2014).
11. Culebras, M., Gómez, C. & Cantarero, A. Enhanced thermoelectric performance of PEDOT with different counter-ions optimized by chemical reduction. *J. Mater. Chem. A* **2**, 10109–10115 (2014).
12. Schultheiss, A. et al. Water content control during solution-based polymerization: a key to reach extremely high conductivity in PEDOT thin films. *J. Mater. Chem. C* **8**, 17254–17260 (2020).
13. Wang, X. et al. High electrical conductivity and carrier mobility in oCVD PEDOT thin films by engineered crystallization and acid treatment. *Sci. Adv.* **4**, eaat5780 (2018).
14. Kim, J. Y., Kwon, M. H., Min, Y. K., Kwon, S. & Ihm, D. W. Self-assembly and crystalline growth of poly(3,4-ethylenedioxythiophene) nanofilms. *Adv. Mater.* **19**, 3501–3506 (2007).
15. Zuber, K., Fabretto, M., Hall, C. & Murphy, P. Improved PEDOT conductivity via suppression of crystallite formation in Fe(III) tosylate during vapor phase polymerization. *Macromol. Rapid Commun.* **29**, 1503–1508 (2008).
16. Fabretto, M., Müller, M., Zuber, K. & Murphy, P. Influence of PEG-*ran*-PPG surfactant on vapour phase polymerised PEDOT thin films. *Macromol. Rapid Commun.* **30**, 1846–1851 (2009).
17. Shi, W. et al. Micron-thick highly conductive PEDOT films synthesized via self-inhibited polymerization: roles of anions. *NPG Asia Mater.* **9**, 405 (2017).
18. Holmberg, K. Surfactants: in *Ullmann's Encyclopedia of Industrial Chemistry* 1–56 (Weinheim: Wiley-VCH, 2019).
19. Kazemi, F. et al. Lanthanide dodecyl sulfates, a potent family of catalysts for the preparation of biobased epoxy thermosets. *Chem. Commun.* **57**, 6784–6787 (2021).
20. Pradhan, K., Paul, S. & Das, A. R. $Fe(DS)_3$, an efficient Lewis acid-surfactant-combined catalyst (LASC) for the one pot synthesis of chromeno[4,3-b]chromene derivatives by assembling the basic building blocks. *Tetrahedron Lett.* **54**, 3105–3110 (2013).
21. Veisi, H. et al. In situ generation of Iron(III) dodecyl sulfate as Lewis acid-surfactant catalyst for synthesis of bis-indolyl, tris-indolyl, Di(bis-indolyl), Tri(bis-indolyl), tetra(bis-indolyl)methanes and 3-alkylated indole compounds in water. *RSC Adv.* **4**, 30683–30688 (2014).
22. Rao, C. R. K., Muthukannan, R. & Adriel Jebin, J. Antony Raj, T & Vijayan, M. Synthesis and properties of polypyrrole obtained from a new Fe(III) complex as oxidizing agent. *Indian J. Chem.* **52A**, 744–748 (2013).
23. de la Iglesia, P. *Structure-Property Relationship of Self-Assembled Conjugated Polymers*. (University of Washington, 2015).

24. Pereira, R. F. P. et al. Structural characterization of solid trivalent metal dodecyl sulfates: from aqueous solution to lamellar superstructures. *RSC Adv.* **3**, 1420–1433 (2013).
25. Lind, M. D. Crystal structure of ferric chloride hexahydrate. *J. Chem. Phys.* **47**, 990–993 (1967).
26. Hartman, M., Trnka, O. & Šolcová, O. Thermal decomposition of aluminum chloride hexahydrate. *Ind. Eng. Chem. Res.* **44**, 6591–6598 (2005).
27. Müller, M., Villalba, J. C. & Anaissi, F. J. Thermal decomposition (TG-DTA) of iron salts [$FeCl_3$.**6**H_2O] and [$Fe(NO_3)_3$.$9H_2O$] with morphologic and chemical analysis of final product. *Semin. Ciênc. Exatas Tecnol.* **35**, 9–14 (2014).
28. Wang, H., Li, Y., Gao, J., Zhang, M. & Guo, M. A novel hydrothermal method for zinc extraction and separation from zinc ferrite and electric arc furnace dust. *Int. J. Miner. Metall. Mater.* **23**, 146–155 (2016).
29. Ali, M. A., Kim, H. H., Lee, C. Y., Soh, H. S. & Lee, J. G. Effects of the $FeCl_3$ concentration on the polymerization of conductive poly(3,4-ethylenedioxythiophene) thin films on (3-aminopropyl) trimethoxysilane monolayer-coated SiO_2 surfaces. *Met. Mater. Int.* **15**, 977–981 (2009).
30. Li, J. X. & Ma, Y. X. Study on fabricating PEDOT electrodes by liquid phase depositional polymerization of EDOT and direct patterning with 172 nm vacuum ultraviolet radiation. *ACS Appl. Energy Mater.* **1**, 134–142 (2018).
31. Gueye, M. N., Carella, A. & Massonnet, N. Structure and dopant engineering in PEDOT thin films: Practical tools for a dramatic conductivity enhancement. *Chem. Mater.* **28**, 3462–3468 (2016).
32. Gueye, M. N., Carella, A., Demadrille, R. & Simonato, J. All-polymeric flexible transparent heaters. *ACS Appl. Mater. Interfaces* **9**, 27250–27256 (2017).
33. Brooke, R. et al. Vapor phase synthesized poly(3,4-ethylenedioxythiophene)-trifluoromethanesulfonate as a transparent conductor material. *J. Mater. Chem. A* **6**, 21304–21312 (2018).
34. Fabretto, M. et al. High conductivity PEDOT resulting from glycol/oxidant complex and glycol/polymer intercalation during vacuum vapour phase polymerization. *Polymer* **52**, 1725–1730 (2011).
35. Chen, S. et al. Unraveling vertical inhomogeneity in vapour phase polymerized PEDOT:Tos films. *J. Mater. Chem. A* **8**, 18726–18734 (2020).
36. Wu, D. et al. Temperature dependent conductivity of vapor-phase polymerized PEDOT films. *Synth. Met.* **176**, 86–91 (2013).
37. Martin, D. C. et al. The morphology of poly(3,4-ethylenedioxythiophene). *Polym. Rev.* **50**, 340–384 (2010).
38. Farka, D., Jones, A. O. F., Menon, R., Sariciftci, N. S. & Stadler, P. Metallic conductivity beyond the Mott minimum in PEDOT: Sulphate at low temperatures. *Synth. Met.* **240**, 59–66 (2018).
39. Fernandez, F. D. M., Khadka, R. & Yim, J. A comparative study between vapor phase polymerized PPy and PEDOT - Thermoplastic polyurethane composites for ammonia sensing. *Polymer* **217**, 123463 (2021).
40. Giffney, T., Xie, M., Sartelet, M. & Aw, K. C. Vapor phase polymerization of PEDOT on silicone rubber as flexible large strain sensor. *AIMS Mater. Sci.* **2**, 414–424 (2015).
41. Zardetto, V., Brown, T. M., Reale, A. & Carlo, A. D. Substrates for flexible electronics: A practical investigation on the electrical, film flexibility, optical, temperature, and solvent resistance properties. *J. Polym. Sci. Part B Polym. Phys.* **49**, 638–648 (2011).
42. Li, Q. et al. Synergistic enhancement of thermoelectric and mechanical performances of ionic liquid LiTFSI modulated PEDOT flexible films. *J. Mater. Chem. C* **7**, 4374–4381 (2019).
43. Stempien, Z., Rybicki, E., Rybicki, T. & Kozanecki, M. Reactive inkjet printing of PEDOT electroconductive layers on textile surfaces. *Synth. Met.* **217**, 276–287 (2016).
44. Tsao, C., Guo, X. & Hu, W. Highly stretchable conductive polypyrrole film on a three dimensional porous polydimethylsiloxane surface fabricated by a simple soft lithography process. *RSC Adv.* **6**, 113344–113351 (2016).
45. Kwak, B. W., Choi, Y. C. & Lee, B. S. Small variations in the sheet resistance of graphene layers with compressive and tensile bending. *Physica E* **68**, 33–37 (2015).
46. Won, S. et al. Double-layer CVD graphene as stretchable transparent electrodes. *Nanoscale* **6**, 6057–6064 (2014).
47. Nguyen, B., Lin, J. F. & Perng, D. Microstructural, electrical, and mechanical properties of graphene films on flexible substrate determined by cyclic bending test. *ACS Appl. Mater. Interfaces* **6**, 19566–19573 (2014).
48. Wang, Y. et al. A highly stretchable, transparent, and conductive polymer. *Sci. Adv.* **3**, e1602076 (2017).
49. Amri, F., Husseinsyah, S. & Hussin, K. Effect of sodium dodecyl sulfate on mechanical and thermal properties of polypropylene/chitosan composites. *J. Themoplast. Compos. Mater.* **26**, 878–892 (2013).
50. Agarwal, V. et al. Influence of anionic surfactants on the fundamental properties of polymer/reduced graphene oxide nanocomposite films. *ACS Appl. Mater. Interfaces* **13**, 18338–18347 (2021).
51. Fu, W. et al. Materials and technologies for multifunctional, flexible or integrated supercapacitors and batteries. *Mater. Today* **48**, 176–197 (2021).
52. Ala, O. et al. Conductive textiles via vapor-phase polymerization of 3,4-ethylenedioxythiophene. *ACS Appl. Mater. Interfaces* **9**, 29038–29046 (2017).
53. Kim, Y. et al. A glucose sensor based on an organic electrochemical transistor structure using a vapor polymerized poly(3,4-ethylenedioxythiophene) layer. *J. Appl. Phys.* **49**, 01AE10 (2010).
54. Koydemir, H. C. & Ozcan, A. Wearable and implantable sensors for biomedical applications. *Annu. Rev. Anal. Chem.* **11**, 127–146 (2018).

Acknowledgements

This research was partly supported by the Basic Science Research Program through the National Foundation of Korea (NRF) funded by the Ministry of Education (2017R1D1A1B03035171), partly supported by the Technology Development Program (C0509911) funded by the Ministry of SMEs and Startups (MSS, Korea), and also partly supported by Flexolution Corporation in Korea. These three different funding sources equally contributed to this work. The authors acknowledge Dr. You Wan Li from the College of Chemistry and Materials, Hunan University of Arts and Science, Chande, China for the semi-empirical energy calculation.

Author contributions

F.M. and S.K. proposed the idea and concept. F.M. carried out most of the work including the preparation, characterization, and measurements of the materials. S.C. prepared the materials for TEM imaging and partly for XRD measurements. D.L. and S.P. performed most of the XRD and XPS measurements and analyses. S.B.J. carried out the preparation, characterization, and measurements of the materials for revision purposes. S.P.C. performed TEM imaging and analysis. J.B. helped with the TEM and XRD analyses. S.K. supervised the project.

Competing interests

F.M. and S.K. have applied for a Korean patent related to the work (10-2224357) through the Flexolution Corporation in Korea. F.M. and S.K. don't have any other competing interests. All the other authors declare that they have no competing interests at all.

Additional information

Supplementary information The online version contains supplementary material available at https://doi.org/10.1038/s41467-024-51621-1.

Correspondence and requests for materials should be addressed to Sungsoo Kim.

Peer review information *Nature Communications* thanks Jean-Christophe Lacroix and the other anonymous, reviewers for their contribution to the peer review of this work. A peer review file is available.